The microstructure and the phase stability of a Cu-30at%Al alloy obtained by reactive milling and quenching

Journal:	*Metallography, Microstructure, and Analysis*
Manuscript ID	Draft
Select "Peer-Reviewed Paper" unless otherwise advised.:	Peer-Reviewed Paper
Date Submitted by the Author:	n/a
Complete List of Authors:	Giordana, Maria Florencia; Centro Atómico Bariloche. CNEA-CONICET , División Física de Metales; Esquivel, Marcelo; Centro Atómico Bariloche. CNEA-CONICET. Av. Bustillo km 9.5, Caracterizacion de Materiales; Universidad Nacional del Comahue Centro Regional Universitario Bariloche, Zelaya, Eugenia; Centro Atomico Bariloche, Materials; Comisión nacional de investigación científica y técnica,
Area of Expertise/Keywords:	Heat Treating, Phase Transformations, Microstructure, Powder Metallurgy, Copper Alloys

The microstructure and the phase stability of a Cu-30at%Al alloy obtained by reactive milling and quenching

M.F. Giordana[a], M.R. Esquivel[b,c], E. Zelaya[b,*]

[a]Instituto de Física de Rosario – CONICET – UNR, Ocampo 210 bis, Rosario 2000, Santa Fe, Argentina.

[b]Centro Atómico Bariloche CNEA-CONICET, Av. Bustillo 9500, Bariloche 8400, Rio Negro, Argentina.

[c]Centro Regional Universitario Bariloche - UNCo, Quintral 1250, Bariloche 8400, Rio Negro, Argentina.[*]zelaya@cab.cnea.gov.ar (E. Zelaya)

The grain growth and the percentage of phases is analized in a Cu-30at%Al powder sample. The phase stability of the quenched sample is analized by using different heat treatments. The evolution of the different phases is studied by in-situ high temperature XRD, transmission electron microscopy and differential scanning calorimetry. The interpretetion of the microstructure obtained for different heat treatmens is focused in the analysis of the γ_2 phase. The grain size of the γ_2 phase, grows more than one order of magnitude when treated from room temperature to 500 °C. However, these grain sizes do not change at isothermal treatments for temperatures values lower than 600 °C. This behavior may be attributed to the pinning resulting from the presence of the nanometric grains of the other phases. The fact that grain size do not grow at a constant temperature is a promising result for the technological applications like shape memory alloys.

Keywords: copper alloys, heat treating, phase transformation, powder metallurgy, microstructure.

Introduction

Eventought the multiple properties of Cu-Al based shape memory alloys (SMA) are reported since 1971 [1], current reviews show the importance of the investigations of new routes for Cu based SMA fabrication [2,3]. Shape memory, pseudoelasticity and two-ways shape memory are properties

present in these alloys between 16at%Al to 30at%Al. All these macroscopic effects are governed by the martensitic transformation (MT).

The Fig. 1 shows the phase diagram of Cu-Al containing the region where the martensitic trasnformation occurs. The black dotted-dash line indicates the temperature where the MT occurs for different Al concentrations. The vertical dashed red line indicates the percentage of Al used in this work. As it could be apreciated in the phase diagram, this first order transformation has a strong dependence on the Al concentration. Moreover, the metastable β_1 phase would transform to either β'_1 or γ' depending on the Al concentration. The β_1 phase is an ordered bcc structure that inherits the lattice parameter of the β phase, being this one a disordered bcc structure [4]. The β'_1 phase could be described as a monoclinic phase i.e. either 9R or 18R with a ABCBCACAB staking sequence [5,6], while the γ' phase could be described as an hexagonal phase or 2H with an AB staking sequence [7]. The MT region is sorrounded by both α and α_2 domain regions at lower Al content and γ_2 domain region in alloys with Al content higher than ~30%. The α phase has a fcc structure with a lattice parameter higher than pure Cu due to the random substitution of Cu by Al. This phase is disordered [4]. Around Cu–23at%Al and below 350 °C, the α_2 phase appears with a tetragonal structure [7,8]. The γ_2 phase has a cubic-based structure with a lattice parameter three times larger than the one of the α phase and the unit cell contains a total of 52 atoms and 2 structural vacancies [9].

The martensitic transformation, either $\beta_1 \leftrightarrow \beta'_1$ or $\beta_1 \leftrightarrow \gamma'$, does not involve the α, α_2 and γ_2 phases. However, different kinds of heat treatments on the quenched samples could hinder the martensitic tranformation due the precipitaction of these phases [10,11]. If the mantersitic transformation is hindered this material could be useless as a SMA. At 30at%Al, the main precipitation process is governed by the γ_2 phase precipitation [10]. Moreover, the high transformation temperature (Ms $\cong$ 200 °C) is the main attractive property of Cu-Al based SMA. This is an advantage over Ti-Ni based SMA. For this reason, it is important to study the precipitation of the γ_2 phase under different heat treatments. Many authors investigate nucleation and gowth of the γ_2 phase in β_1 phase for different Cu-Al based SMA [12-15]. However, most of these works are focused in the study of either single crystals or alloys with large grains.

On one hand, as it is mentioned in the first paragraph, the reactive milling (RM) is a technique involved in the possible routes of new fabrication methods of SMA. The RM could reduce the grain size improving the ductility of the final compacted powder [2,16,17]. In the wok of Vajpai et. al., it is shown that Cu-Al-Ni SMA strip could be prepared using alloyed powders by hot densification rolling of unsheathed sintered powder preforms [16]. These strips with a 16 nm average grain size have a high strength average fracture stress ≅ 810 MPa and ductility. In addition, in this work, the straightforward relationship between the final particle size obtained in the milling process and the grain size after the final quenching step is pointed out. On the other hand, it should be mentioned that both the final grain and particle size are directly related to the milling stage achieved for each composition [18]. In addition, the Cu-Al intermetallics do not reach necessarily the phase equilibrium of the phase diagram for each composition [18]. Moreover, other authors showed that after milling times larger than 4 hours or after a heat treatment at 300 °C the milled sample evolves to nanometric crystals of γ_2 phase [19,20]. For these two reasons and in order to achieve a SMA with a high strength and ductility, it is important to investigate the phase stability of the powders, the percentage of phase and the grain size evolution for different heat treatments. The first point was already performed in [21]. In that work, it is shown that the phase stability for Cu-24at%Al of two samples obtained by two different milling methods is not the same. However, not many authors study neither the microstructure evolution (in terms of grain size) nor the percentage of phase evolution for different heat treatments.

The aim of this work is to investigate the phase stability of potential SMA Cu-30at%Al obtained by RM and then quenched from 850 °C. This investigation not only shows the evolution of the different phases by in-situ high temperature XRD (HT-XRD), transmission electron microscopy (TEM) and differential scanning calorimetry (DSC) but also analyzes the difussion in terms of the grain growth and the phase percentage at different temperatures and under different heat treatments. .

Materials and methods

Elemental Cu (Sigma-Aldrich, 99.999 % purity, 5 mesh) and Al (Alfa-Aesar, 99.5 % purity, 100 mesh) powders in ratio Cu-30at%Al are mechanically alloyed. The milling process is carried out for 50 h in a Fritsch pulverissette 6 planetary-motioned mill. The selected milling speed is 120 rpm. The ball/sample mass ratio is 8.25:1. The milling process is performed at controlled conditions

(humidity\100 ppm, O_2 content\5 ppm). The as-milled powder is heat treated by sealing it in a quartz capsule under an Ar atmosphere and annealing in an ad-hoc designed laboratory oven. The heat treatment consisted of annealing at 850 ºC for 48 h followed by water quenching.

The quenched sample is characterized using both a TEM FEI TECNAI F20 G2 field emission and a Philips CM200 UT microscopes operated at 200 keV. The thermal stability of the quenched sample is studied by differential scanning calorimetry (DSC 2970, TA instruments). The measurements are taken between room temperature and 500 ºC in a purified Ar (purity 99.999 %) atmosphere at a heating rate of 5 ºC min^{-1}. The phase stability of the quenched sample is also studied by in situ HT-XRD using an Anton Paar HTK 1200 N chamber with an automatic height-Z correction connected to a PANalytical Empyrean diffractometer with PixCel 3D detector. In the first thermal treatment, the isothermal measurements at selected temperatures are performed with a heating program from room temperature to 700 ºC using a 10 ºC min^{-1} heating ramp under a He (purity 99.999 %) flow of 100 ml min^{-1}. During heating, selected temperatures are chosen to obtain the difractograms at: 25 ºC, 200 ºC, 250 ºC, 280 ºC, 300 ºC, 320 ºC, 350 ºC, 380 ºC, 400 ºC, 450 ºC, 500 ºC, 550 ºC, 600 ºC, 700 ºC. Each diffractogram at each temperature is is done for one hour. High statistic XRD profiles are analyzed with the Rietveld method using the Fullprof software. This method is used to calculate grain size [22, 23]. In this work the term “grain size” will be used as a synonym of crystallite domain. The phase composition is calculated according to a method presented elsewhere [21, 24]. The second, third and fourth heat treaments are isothermal measurements at: 350 °C, 550 °C and 700 °C, respectively. In all these heat treaments a diffractogram is obtained at: 0 h, 2 h, 3.5 h, 5 h, 8 h 11 h and 18 h. The Fig. 2 sumarizes the previous steps done before this work and all the heat treatments done in this work. The results and analisys of the milling process were discussed in other works (ligth blue and dark yelow posting signs in Fig. 2). In this work, the results of the heat treatments performed over the milled and quenched sample are analized (green posting signs in Fig. 2). The quenching is performed in order to retain the larger amount of the β phase. The larger the porcentage of the β phase in the quenched alloy, the larger amount of the MT in the sample and the better the performance of the SMA. Eventhought the β phase retained is not expected to have the largest mass percentage of the sample due to the powder characteristics, this analysis is a first original and

unreported approach to understand the relation between heat treatment, grain size and martensitic transformation in Cu30at%Al uncompresed powder alloys.

Results and discusion

The diffractogram of the sample before any heat treatments is shown in Fig. 3 in order to organize and describe the different heat treatments done to the Cu-30at%Al sample milled and quenched. Moreover, the calorimetric evolution of this sample and one diffractogram of the first heat treatment is shown as an introduction. This organization will show the reader the motivation beneath each heat treatment and the analysis of the results.

Before the quenching from 850 °C, the milled powder is mainly of a mixture of the α and the γ_2 phases [25]. After the quenching, the room temperature XRD of the sample is indexed considering the two stable phases for this composition: α_2 and γ_2 as shown in Fig. 3a. The calorimetric evolution of this last sample is shown in Fig. 3b. Two wide global exothermal events are observed. These events occur between 190 °C ± 2 °C and 425 °C ± 2 °C. To understand the processes related to the calorimetry events, in-situ HT-XRD measurements are performed at different temperatures. In particular, Fig. 3c shows the diffractogram obtained at 500 ºC. It is indexed as a mixture of the α, the γ_2 and the β_1 phases denoting the occurrence of more than one phase transformation.

The next section show the %mass amount evolution of each phase at different temperatures. A XRD measurement similar to the one showed in Fig. 3c is performed at different temperatures.

First heat treatment

The HT-XRD indexation for each temperature is summarized in Table 1. At room temperature, the present phases are the α_2 and the γ_2. As the temperature increases, a martensitic phase appears: the β_1'. At 300 ºC, the martensitic transformation from the β_1' to the β_1 ordered phase starts and continues up to 380 ºC, when the martensitic phase is no longer observed. At this temperature, the transformation from the α_2 to the α phase also ocurrs as predicted by the equilibrium diagram shown in Fig.1. Finally, at 500 ºC the β_1 ordered phase transforms to the high-temperature disordered β phase. At temperatures higher than 600 ºC, the cubic α phase is not detected any longer.

The evolution of the phases is also clearly observed in Fig. 4. Both figures show the mass porcentage of phases as a function of temperature. The mass percentage is obtained according to the method used previously in N.N. Sanchez Pascal et al. [21]. The same method is used elswhere [24]. The results are separated in two graphics in order to analyze the behaviour of each group of phases. It is thoroughly observed that the γ_2 is the major phase up to 600 ºC, representing in most cases an average mass percentage larger than 70 %. Eventhough the total amount of the γ_2 seems to slowly decrease up to 600 ºC, some changes in the slopes could be appreciated when the β_1, the α and the β phases nucleate. Other important result obtained from these curves is that both the α_2 to the α (Fig. 4a) and the β'_1 to the β_1 (Fig. 4b) transformations occur while maintaining a similar mass percentage when transforming from one phase to the other. However, when the nucleation of the β phase occurs not only the α phase disappear but also the γ_2 phase decreases drastically. In other words, the β'_1 and the β_1 phases do not increase significantly. On the contrary, the β phase eliminates the α one and the γ_2 phase decreases drastically. The evolution of the phases seems to obey the tendency shown in the phase diagram for a composition near 30at%Al (Fig. 1). Moreover, this result explains the calorimetric events involved in the two subsequent processes, first the martensitic transformation of the β_1' to the β_1 and second the transformation of the α_2 to the α. However, the process seems to occur in a wider temperature range in this sample than in those elaborated by fusion [26, 27]. One possible explanation of this fact could be a large difference in grain sizes. Moreover, it is interesting to obtain the evolution of the microstructure of the quenched powders. In particular, the evolution of grain size of the γ_2 phase. This evolution would help to understand if the large contribution is sustained by the increment of the grain size or the increment of the total phase per se.

The Fig. 5 shows the grain size (D) corresponding to the indexed phases as a function of the temperature. The statistical error calculated for the average grain size ranges are from 2 % to 10 %. The obtained values are presented in two different graphs in Fig. 5 in order to clearly show the phase transformations as the temperature increases. At 25ºC, the phases indexed are both α_2 and γ_2, with an average grain size of 26 nm and 145 nm, respectively. The D value corresponding to the phase α_2 increases slightly before completely transform reaching a value near 42 nm. The α_2 transformation results in the appearance of the α phase with D = 49 nm, and as in the previous case, the grain size

increases up to 550 °C reaching a value of 198 nm. At 300 °C the phase β_1 appears with a D value equal to 30 nm, and reaches 64 nm at a temperature of 500 °C. At higher temperatures, the transformation to the β phase occurs. For this structure, the size of grain increases from 74 nm to 138 nm.

The γ_2 phase is one of the most important crystalline structure for the composition studied in this article, since it is the main one at the different temperatures. The first notorious result is the decrement in grain size when a new phase nucleates. In Fig. 5, the formation of new phases is labelled with vertical dotted lines in order to easily visualize the relationship between these formations and the decay in the grain size of the γ_2. Clearly, the driving force of the nucleation of each new phase hinders the growth of the γ_2 crystals. The second unexpected result is the growth of the γ_2 phase grain. From the studies carried out for microstructure, it is clear that the γ_2 phase exhibits the largest grain size increment, changing in more than an one order of magnitude (from 145 nm to 2282 nm). This change of the grain size in more than one order of magnitude seems to be a problem for a possible technological application. If the grain size increases more than one order of magnitude at different temperatures, probably the evolution of the γ_2 phase at a same temperature for long periods, also increases the grain size of the γ_2 phase. This behavior hinders the martensitic transformation and inhibit the potential application as a SMA. Moreover, it is already reported as a problem for single crystals [14]. For this reason, it is important to analyze the evolution of the γ_2 phase at a constant temperature for a long period of time.

Second and third heat treatment

The γ_2 phase growth from the β phase seems to clearly hinder the martensitic transformation at 200 °C [14]. Therefore, a treatment temperature of 350 °C is selected to obtain a curve accurate enough of the grain size as a function of the treatment time. This curve will allow the measurement of the kinetics of the grain size grow according to Porter and Easterling [28]. However, at this temperature the first diffractogram does not differ from the one taken after 18 h of thermal treatment at the same temperature within the experimental errors. For this reason and taking into account that the γ_2 phase

is dominant at temperatures lower than 600 °C, a higher temperature is selected to measure the kinetics of the grain size growth.

The Fig. 6 shows the diffractogram of the Cu-30at%Al sample after milling and quenching at 550 °C and the diffractogram of the same sample after 18 h at 550 °C. Again, no change is observed within the experimental errors. These results indicate that at this temperature the driving force and the grain boundary mobility is not large enough to promote a change in grain size. Eventhough the grain size of the γ_2 grows one order of magnitude with temperature, once the grain reach a determine size, it does not grow at that temperature as time goes by. The nanometric crystals of the α and the β phases could act as attachment points that inhibit the grain growth of the γ_2 phase and vice versa. To determine if there is a temperature that activates the grain boundary mobility, a heat treatment at 700°C is selected.

Fourth heat treatment

The Fig. 7a shows the evolution of two peaks of the diffractogram of the Cu-30at%Al sample after milling and quenching at 700 °C during 18 h. Here, a significant change in the main peaks of the diffractogram is appreciated. Moreover, the average grain size of the γ_2 and the β phases shows an evolution with the time at 700 °C as presented in, Fig. 7b. Also, note that since this experiment starts with a quenched sample the sizes of grains are rather different from the ones presented in Fig. 5b. The average grain size as a function of time has a behavior predicted by Porter and Easterling [28] until 12 h is reached. The moving boundaries of the γ_2 phase seem to be attached by the presence of the β phase particles, so that the particles exert a pulling force on the boundary by restricting its motion. This pulling force opposes to the driving force for the grain growth. In other words, the other phases act like pinning to the growth of the γ_2 phase. The result of the competition of this opposite forces describes a mean diameter grain size grow as a function of time according to: $D=Kt^n$, where D is the mean diameter of the grain size, K a constant, t the time and $n < 0.5$. Moreover, the grain growth in the presence of a second phase achieves a maximum value of r/f, where r is the mean grain radius without considering the presence of a second phase and f is the fraction value. However, after 12 h the main grain diameter reaches even higher values. This behavior could be attributed to the dissolution of the smallest β phase crystals. However, after 12 h at 700°C the percentage of the

β phase is 0.78 while after 18 hours at 700°C the percentage of the β phase is 0.81. Also, the mean grain size of the β phase particles seems to not decrease. the presence of grains of sizes below the detection limit of the XRD technique could be one possible explanation of this behavior and to the lack of the grain growth until temperatures higher than 600 °C are reached. The TEM technique is used in order to detect the presence of the nanometric domains in this sample.

TEM analysis

The TEM analysis allows to study the micro and nano structure of the samples. All samples are powders composed of micrometric particles constituted by nanometric grains. One of the most suitable TEM technique to measure grain sizes is dark field imaging. In the case of the sample before annealing and quenching, the mean grain size is 18 nm with a dispersion equal to 14 nm [18]. The Fig. 8 shows one particle of the sample after quenching. The Fig. 8a corresponds to the bright field of the particle and the Fig. 8b and c are two different dark field images. In this case, there is a large dispersion on the grain sizes, it is possible to measure grains from 4 nm (the smallest in Fig. 8b, indicated with a red arrow) to more than 50 nm (the largest in Fig. 8c, indicated with a red arrow). These values seem to be lower than the grain size measured by XRD for the α_2 equal to (25 ± 3) nm and for γ_2 equal to (145 ± 15) nm. However, this difference could be due to the limitation of the XRD techniques used in this work to detect grain sizes smaller than 20 nm [29]. Moreover, dark field images allow to detect grain sizes as small as 3 nm [30]. The lack of detection of grain lower than 20 nm would easily explain the difference of mean grain size between both techniques. Moreover, the presence of grain as small as 4 nm would explain the lack of grain mobility at temperatures lower than 600 °C. The crystal growth inhibition by the second-phase particles was already reported by other authors like: “Zener pinning” or “Zener drag” [31]. The effect produces that the smaller crystals act as pins that inhibit the bigger grain boundaries mobility. The higher the difference of grain size or the percentage of smaller crystals the higher the Zener effect. At higher temperatures (~ 700 °C) the pulling force of the nanometric crystals is overcome by the grain boundary mobility activated by temperature. Once the pining effect is overcome the γ_2 phase seems to be the major phase once again. This effect is clearly observed for times longer than 15 hours in Fig. 7b.

Finally, it should be remarked that eventhough the grain size of the γ_2 phase increase with temperature (Fig. 4), at a constant working temperature, the difference of grain sizes favors the Zener effect. The Zener pinning created by the nanometric crystals inhibits the γ_2 phase growth (Fig. 6 and Fig. 7). The presence of such small grain is a very promising since this kind of alloys could be useful like shape memory alloys for working at temperatures near 200 °C [32].

Conclusions

The phase stability of a potential SMA Cu-30at%Al milled and quenched is studied at room temperature, 350 °C, 550 °C and 700 °C. The phase stability at different temperatures is analized in terms of the microstructure (grain growth) and the phase percentage.

The decrement in grain size of the γ_2 phase is observed every time a new phase nucleates. The most notorious result is the increment of the γ_2 phase grains in more than one order of magnitude (from 145 nm to 2282 nm). However, the size of the γ_2 phase grains do not change at a constant temperature with the time at temperatures lower than 600 °C. This behavior could be attributed to the pulling force resulting from the presence of nanometric grains.

The lack of grain size growth at a constant temperature is a promising result for the technological application of this kind of SMA materials.

Acknowledgments

The authors thanks to Consejo Nacional de Investigaciones Científicas y Técnicas (CONICET), to the Agencia Nacional de Promoción Científica y Tecnológica (ANPCyT: PICT-2015-1641), to Comisión Nacional de Energía Atómica (CNEA) and to Universidad Nacional del Comahue (UNCo: PI-B202-2017) for the financial support to this work.

Bibliography

[1] K. Oishi, L.C. Brown, Metallurgical Transactions Volume 2, Issue 7 (1971) 1971-1977.

[2] A. Agrawal, R.K. Dube Journal of Alloys and Compounds 750 (2018) 235-247.

[3] R. Dasgupta, Journal of Materials Research Volume 29, Issue 16 (2014) 1681-1698.

[4] J.L Murray, International Metals Reviews Volume 30, Issue 1 (1985) 211-233.

[5] G. Roulin, P. Duval, Initial stages of ordering obtained by tempering of disorder martensitic phase of Cu–Al alloys, Scr. Mater. 37 (1997) 45–51.

[6] Z. Nishiyama, J. Kakinoki, S. Kajiwara, J. Phys. Soc. Jpn. 20 (7) (1965) 1192–1211.

[7] P.R. Swann, H. Warlimont, Acta Metall. 11 (6) (1963) 511–527.

[8] G. Roulin, P. Duval, Scr. Mater. 37 (1997) 45–51.

[9] S. Westman, Acta Chemica Scandinavica 19 (1965) 1411-1419.

[10] S.W. Husain,M.S. Ahmed, I. Qamar, Metallurgical and Materials Transactions A, 30 (6) (1999) 1529-1534

[11] G.J. Arruda, A.T. Adorno, R. Magnani, C.R.S. Beatrice. Materials Letters 32 (2-3) (1997) 79-84.

[12] M.L. Castro, R. Romero, Materials Science and Engineering A 287 (1) (2000) 66-71.

[13] M. L. Castro, O. Fornaro, J. Mater. Sci. 44 (2009) 5829–5835.

[14] V.E.A. Araujo, R. Gastien, E. Zelaya, J.I. Beiroa, I. Corro, M. Sade, F.C. Lovey, Journal of Alloys and Compounds 641 (2015) 155–161.

[15] M.T. Ochoa-Lara, H. Flores-Zúñiga, D. Rios-Jara, J Mater Sci 41 (2006) 5455–5461.

[16] S.K. Vajpai, R.K.Dube, S.Sangal, Materials Science & Engineering A 570 (2013) 32–42.

[17] S. Pourkhorshidi, N.Parvin, M.S.Kenevisi, M.Naeimi, H.Ebrahimnia Khaniki, Materials Science & Engineering A 556 (2012) 658–663.

[18] M.F. Giordana, M.R. Esquivel, E. Zelaya, Metallogr. Microstruct. Anal. (2017) 6:139–149.

[19] K. Chittineni, D.G. Bhat, Materials and Manufacturing Processes, 21:5(2006) 527-533

[20] S. Xi, J. Zhou, D. Zhang, X. Wang, Materials Letters 26 (1996) 245-248.

[21] N.N. Sanchez Pascal,M.F. Giordana,F. Napolitano,M.R. Esquivel,E. Zelaya, Advanced Powder Technology 28(10) (2017) 2605-2612.

[22] J. Rodriguez-Carvajal, Proc. Of Fifteenth Conference of the International Union of Crystallography, Tolouse, France, Vol. 127 (1190).

[23] J. Rodriguez-Carvajal, Recent developments of the program FULLPROF, Comm. Powder Diffr. (IUCr) 26 (2001) 12–19.)

[24] J. Kwarciak, Z. Bojajarski, H. Morawiec, Journal of Materials Science 21 (1986) 788-792.

[25] M.F. Giordana, M.R. Esquivel, E. Zelaya, Advanced Powder Technology 26(2) (2015) 470–477.

[26] X.J. Liu , I. Ohnuma, R. Kainuma, K. Ishida, Journal of Alloys and Compounds 264 (1998) 201–208.

[27] H. Cheniti, M. Bouabdallah, E. Patoor, Journal of Alloys and Compounds 476 (2009) 420–424.

[28] D.A. Porter, K.E. Easterling, Phase Transformations in Metals and Alloys (1992) Springer-Science+Business Media, B.Y.

[29] A. Guinier, D.L. Dexter, X-Ray Studies of Materials (1963) Interscience Publishers.

[30] M. De Graef, Introduction to Conventional Transmission Electron Microscopy (2002) Cambridge University Press.

[31] M.M. Moshksar, H. Doty, R. Abbaschian, Intermetullics 5 (1997) 393 399.

[32] R. Dasgupta, Journal of Materials Research 29(16) (2014) 1681-1698.

Figure 1. The Cu – Al phase diagram. The vertical red dash line shows the composition of the alloy analyzed in this work.

Figure 2. The scheme of the process and analisis of the Cu-30at%Al sample.

Figure 3. a. Diffractogram of the Cu-30at%Al sample after milling and quenching measured at room temperature. b.Calorimetric measurement of the sample milled and quenched. c. Diffractogram of the Cu-30at%Al sample after milling and quenching measured at 500 °C by HT-XRD.

Figure 4. Evolution of the average mass % of the Cu-30at%Al milled and quenched sample as a function of temperature. Each point represents a sample mass percentage calculated on each in-situ HT-XRD measurement. The sample mass is calculated according to [21, 24].

Figure 5. The average grain size as a function of the heat temperature of the Cu-30at%Al milled and quenched. Each point represents the analysis done by the Rietveld method [22, 23] to each HT-XRD measurement.

Figure 6. a. Diffractogram of the Cu-30at%Al sample after milling and quenching at 550 °C as received and after 18 h at 550 °C. b. Detail of the larger peaks, no difference is appreciated.

Figure 7. a. Detail of the larger peaks of the diffractogram of the sample Cu-30at%Al after milling and quenching at 700 °C for different times. b. The grain size as a function of the heating time at 700 °C. The grain size is obtained by the Rietveld method [22, 23].

Figure 8. a. Bright field image of the Cu-30at%Al sample milled and quenched. b. and c. Dark field images of the same sample showing the smallest and largest grain sizes in the sample.

Table 1. The phases detected at each temperature by in-situ HT-XRD of the milled and quenched Cu-30at%Al sample in the 25 °C to 700 °C temperature range.

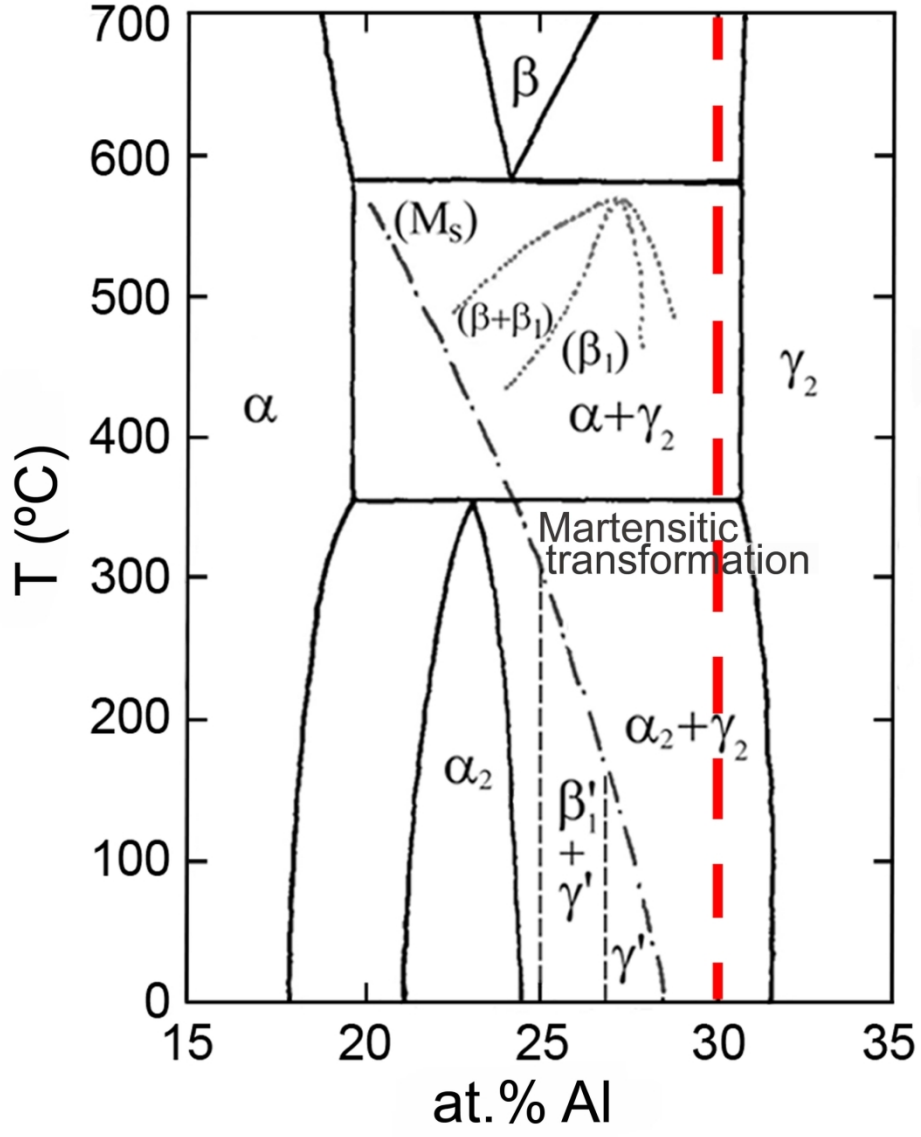

Figure1. The Cu – Al phase diagram. The vertical red dash line shows the composition of the alloy analyzed in this work.

85x98mm (600 x 600 DPI)

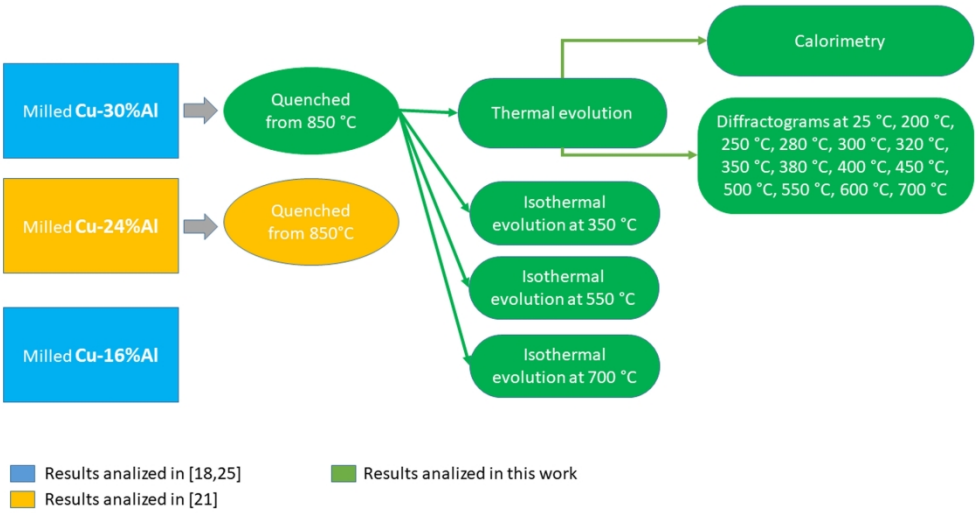

Figure 2. The scheme of the process and analisis of the Cu-30at%Al sample.

149x84mm (600 x 600 DPI)

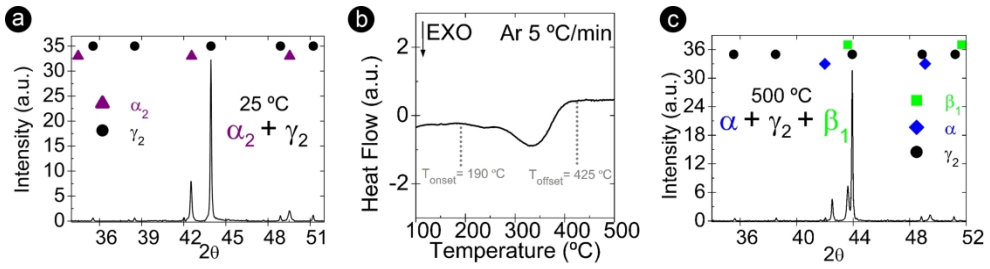

Figure 3. a. Diffractogram of the Cu-30at%Al sample after milling and quenching measured at room temperature. b.Calorimetric measurement of the sample milled and quenched. c. Diffractogram of the Cu-30at%Al sample after milling and quenching measured at 500 °C by HT-XRD.

149x38mm (600 x 600 DPI)

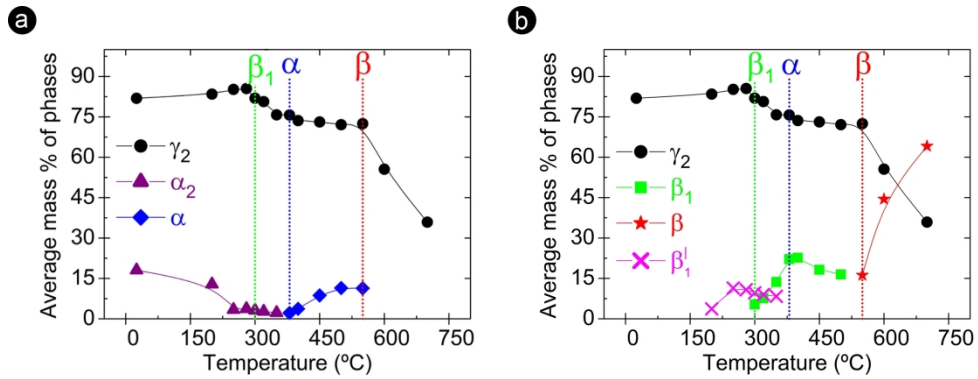

Figure 4. Evolution of the average mass % of the Cu-30at%Al milled and quenched sample as a function of temperature. Each point represents a sample mass percentage calculated on each in-situ HT-XRD measurement. The sample mass is calculated according to [21, 24].

139x52mm (600 x 600 DPI)

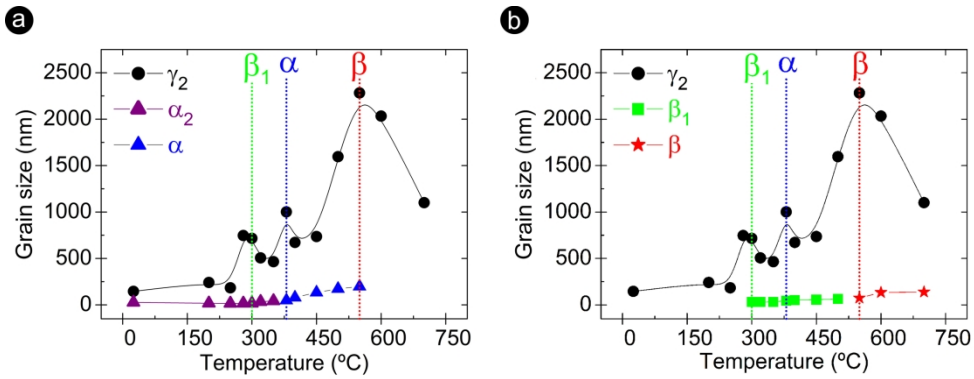

Figure 5. The average grain size as a function of the heat temperature of the Cu-30at%Al milled and quenched. Each point represents the analysis done by the Rietveld method [22, 23] to each HT-XRD measurement.

139x52mm (600 x 600 DPI)

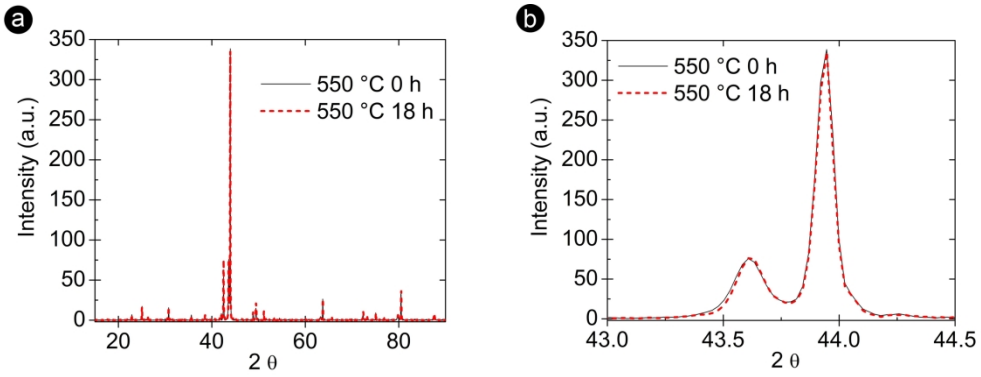

Figure 6. a. Diffractogram of the Cu-30at%Al sample after milling and quenching at 550 °C as received and after 18 h at 550 °C. b. Detail of the larger peaks, no difference is appreciated.

139x52mm (600 x 600 DPI)

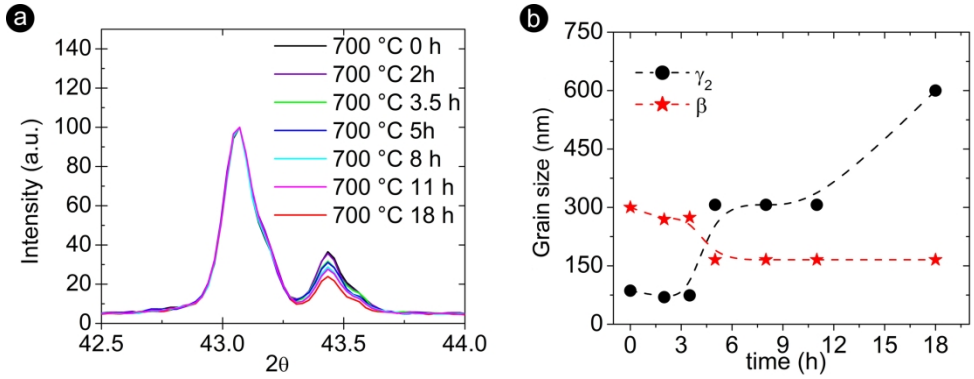

Figure 7. a. Detail of the larger peaks of the diffractogram of the sample Cu-30at%Al after milling and quenching at 700 °C for different times. b. The grain size as a function of the heating time at 700 °C. The grain size is obtained by the Rietveld method [22, 23]

139x52mm (600 x 600 DPI)

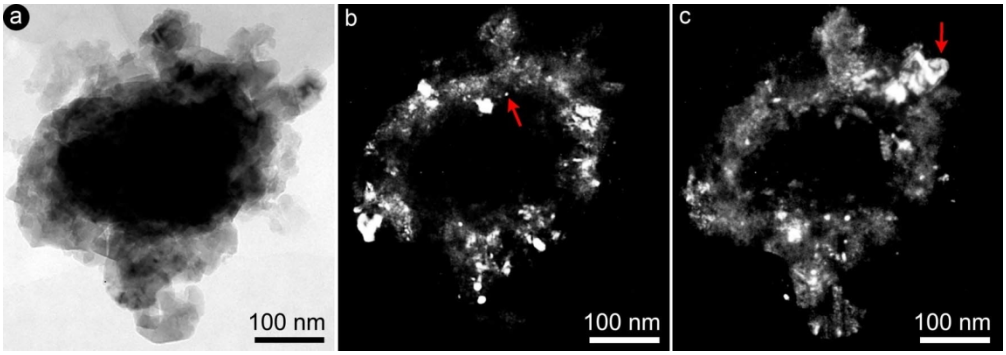

Figure 8. a. Bright field image of the Cu-30at%Al sample milled and quenched. b. and c. Dark field images of the same sample showing the smallest and largest grain sizes in the sample.

150x51mm (300 x 300 DPI)

Table 1. The phases detected at each temperature by in-situ HT-XRD of the milled and quenched Cu-30at%Al sample in the 25 °C to 700 °C temperature range.

XRD temperature	Phases detected by XRD					
25 °C		α_2	γ_2			
200 °C		α_2	γ_2	β_1'		
250 °C						
280 °C						
300 °C		α_2	γ_2	β_1'	β_1	
320 °C						
350 °C						
380 °C	α		γ_2		β_1	
400 °C						
450 °C						
500 °C						
550 °C	α		γ_2			β
600 °C			γ_2			β
700 °C						